Dalton Transactions

Accepted Manuscript

ROYAL SOCIETY OF CHEMISTRY

www.rsc.org/dalton

Ligand Effects on the Electrochemical Behavior of $[Fe_2(CO)_5(L)\{\mu\text{-}(SCH_2)_2(Ph)P{=}O\}]$ ($L = PPh_3$, $P(OEt)_3$) Hydrogenase Model Complexes

Laith R. Almazahreh, Wolfgang Imhof, Jean Talarmin, Philippe Schollhammer, Helmar Görls, Mohammad El-khateeb and Wolfgang Weigand.

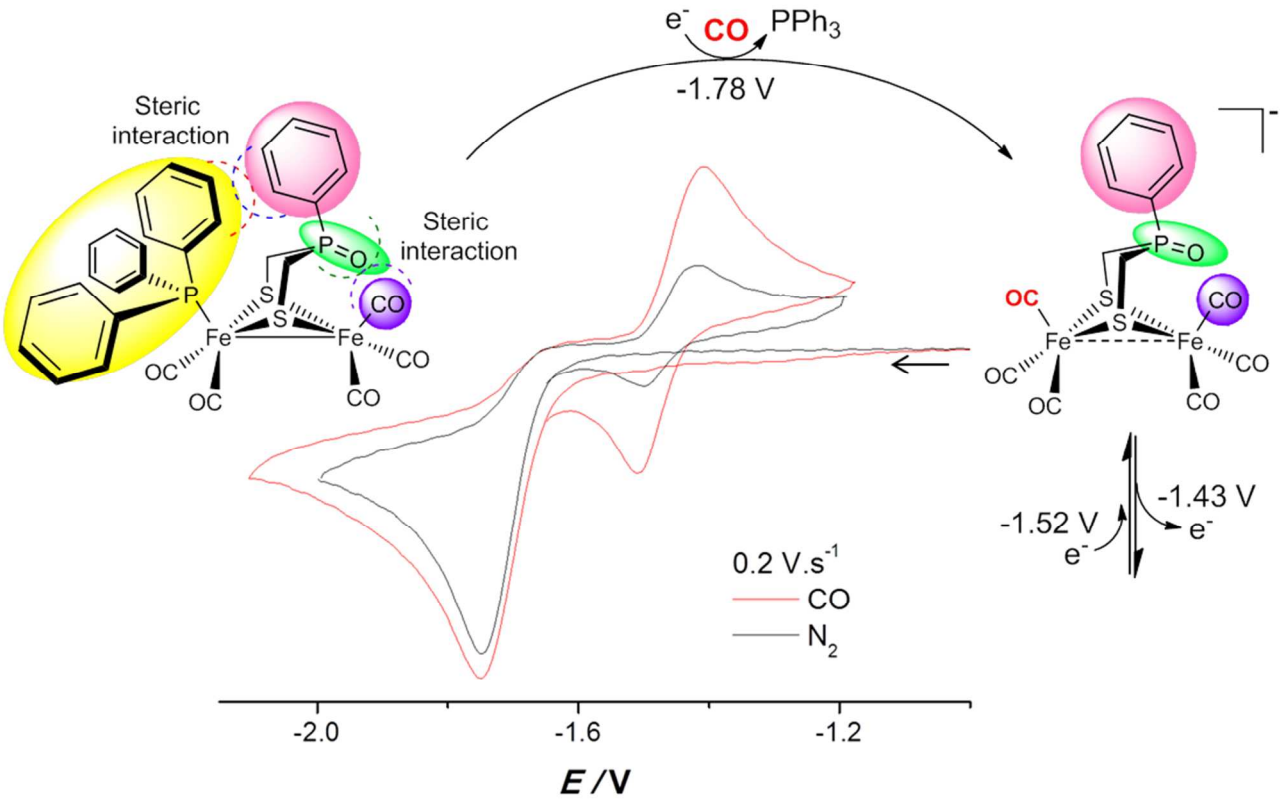

Ligand Effects on the Electrochemical Behavior of $[Fe_2(CO)_5(L)\{\mu\text{-}(SCH_2)_2(Ph)P{=}O\}]$ ($L = PPh_3$, $P(OEt)_3$) Hydrogenase Model Complexes

Laith R. Almazahreh,[†] Wolfgang Imhof,[,‡] Jean Talarmin,[*,£] Philippe Schollhammer,[*,£] Helmar Görls,[†] Mohammad El-khateeb,[⊥] and Wolfgang Weigand[*,†]*

[†]*Institut für Anorganische und Analytische Chemie, Friedrich-Schiller-Universität Jena, Humboldtstrasse 8, D-07743 Jena, Germany,*

[‡]*Institut für Integrierte Naturwissenschaften, Universität Koblenz-Landau, Universitätsstr. 1, D-56070 Koblenz, Germany,*

[£]*UMR CNRS 6521, , Université de Bretagne Occidentale, 6 avenue Le Gorgeu,, C.S. 93837, 29238 Brest-Cedex, France and*

[⊥]*Chemistry Department, Jordan University of Science and Technology, 22110 Irbid, Jordan.*

AUTHOR EMAIL ADDRESS (wolfgang.weigand@uni-jena.de)

RECEIVED DATE (to be automatically inserted after your manuscript is accepted if required according to the journal that you are submitting your paper to)

[*] To whom correspondence should be addressed. E-mail: wolfgang.weigand@uni-jena.de (W.W.), Fax: +49 3641 948102, Tel: +49 3641 948160

Abstract:

In this paper we study the influence of substituting one CO ligand in $[Fe_2(CO)_6\{\mu\text{-}(SCH_2)_2(Ph)P{=}O\}]$ (**1**) by better σ-donor L ligands affording $[Fe_2(CO)_5(L)\{\mu\text{-}(SCH_2)_2(Ph)P{=}O\}]$ {L = PPh_3 (**2**) and $P(OEt)_3$ (**3**)} in relation to the steric interactions and the voltammetric behavior. Cyclic voltammetric investigations under N_2 and CO showed remarkable differences in the electrochemical behaviour of complexes **2** and **3**: (*i*) Complex **2** tends to expel PPh_3 upon reduction whereas complex **3** exhibits chemical reversibility and (*ii*) Under CO, complex **3** reacts with CO affording a new compound **P**, which shows a reversible wave at $E_{1/2}$ ~ -0.9 V (vs ferrocenium/ferrocene couple). The presence of CO assists the formation of **1** after electrochemically induced loss of PPh_3 during the voltammetric experiment of **2**. Using DFT calculations we provide an explanation for the difference in stabilities between the Fe-PPh_3 and Fe-$P(OEt)_3$ bonds.

Keywords: Phosphine oxide/ substitution/ steric effect/ hydrogenase

Introduction

[FeFe]-hydrogenases are enzymes that have high efficiency (ca. 10^4 turnover·s^{-1})[1,2] to catalyze reduction of protons to form dihydrogen.[2,3] This process occurs in microorganisms at neutral pH and a potential of -0.42 V (vs NHE).[4,5] The high resolution X-ray crystallographic and IR spectroscopic studies revealed that the active site of [FeFe]-hydrogenases (so-called H cluster),[6] isolated from *Clostridium pasteurianum*[7] and *Desulfovibrio desulfuricans*[8], consists of a $[Fe_4S_4]$ cluster attached through a cysteinyl residue to a butterfly $[Fe_2S_2]$ subcluster (Figure 1). The coordination sphere of the iron centres of the $[Fe_2S_2]$ subcluster contains biologically unusual CO and CN^- ligands. These iron centres are bridged most likely by the azadithiolate ligand -SCH_2NHCH_2S-.[9] On the functional side of the active site, the protonation of the $[Fe_2S_2]$ subcluster is a central step during the turnover.[10] In addition, the NH group of the azadithiolate is alleged to relay protons to and from the diiron core via agostic or hydrido-proton interaction.[11] The steric bulk at the proximal Fe atom assists the N-H bond (in green, Figure 1) to be in close proximity to the vacant site.[12]

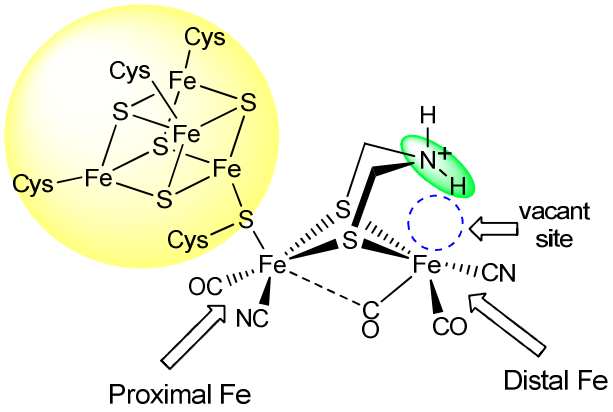

Figure 1. The structure of the H cluster.[6-8]

The high catalytic efficiency and low energy features were the impetus to chemists and engineers for paving the way to macroscale hydrogen production, based on designing of inexpensive electrocatalysts resembling the structure of the H cluster. Numerous model complexes have been synthesized based on replacing the propane dithiolate bridge in $[Fe_2(CO)_6\{\mu\text{-}(SCH_2)_2CH_2\}]$[13] by linkers containing heteroatoms in the bridgehead such as N[14], O[15], S[16], Se[17] and Si[18] to study their influence toward the protonation properties as well as the electrochemical behaviour of the model complex in the absence and presence of acids. In addition, the synthetic chemistry involved substitution of the CO ligands in $[Fe_2(CO)_6\{\mu\text{-}(SCH_2)_2X\}]$ (X = CH_2, NR, O, SiR_2) by cyanide[18b,19], phosphanes[15a,20], phosphites[20], carbenes[20a,20c,21], nitrosyl[22] or sulfides[23]. Mono-, di-, tri- and tetrasubstituted model complexes have been described.[16a,16b,18b,19-23] A basic aim of these substitution reactions was to increase the electron richness at the $[Fe_2S_2]$ core of the model complex in order to mimic the electronic characteristics of the $[Fe_2S_2]$ core of the H-cluster, which contains strong electron donating CN^- ligands. The enhanced basicity of the $[Fe_2S_2]$ core of the substituted models resulted in formation of hydride species prior to reduction, but only in the case of the di-, tri-, or tetra-substituted complexes with strongly electron donating substituents such as PMe_3.[20l,24] Substitution of CO ligands with stronger σ-donors ligands increases not only the electron density at the iron sites, but also at the other protonation sites of the model complex.[20l,24,25] For example, 4 equiv of triflic acid were required to fully protonate the amine group in the hexacarbonyl complex $[Fe_2(CO)_6\{\mu\text{-}(SCHMe)_2NH\}]$, while only 1 equiv was enough in

case of the substituted complex $[Fe_2(CO)_4(PMe_3)_2\{\mu\text{-}(SCHMe)_2NH\}]$.[25] Moreover, Rauchfuss, Zampella and coworkers have recently described the synthesis and protonation kinetics of highly basic PMe_3-tetrasubstituted complexes $[Fe_2(CO)_2(PMe_3)_4\{\mu\text{-}(SCH_2)_2X\}]$ (X = CH_2 and NH) and $[Fe_2(CO)_2(PMe_3)_4\{\mu\text{-}(SCH_2)_2\}]$, which showed S-protonation at low temperatures.[20l] Mimicking the rotated structure of the H cluster has been always a fundamental aim in the synthetic chemistry of the model complexes. Very recently, two research groups reported the first model complexes adopting fully rotated $Fe(CO)_3$ with respect to $Fe(CO)_2$(bis-phosphine) unit and featuring a semi-bridging CO ligand.[26a,b] The two groups described that the rotated structure of $[Fe^IFe^I]$ models can be stabilized by: (*i*) the presence of steric bulkiness on the dithiolate linker, (*ii*) desymmetrization of the coordination environment of the two Fe atoms and (*iii*) the presence of agostic Fe···HC bonding.[26a,b]

We have recently described the synthesis of the model complex $[Fe_2(CO)_6\{\mu\text{-}(SCH_2)_2(Ph)P{=}O\}]$ (**1**), which offers protonation site at the P=O functionality as it undergoes clean and reversible protonation/deprotonation processes using $HBF_4{\cdot}Et_2O$ and Et_3N in CH_2Cl_2 solution.[27] In addition to the protonation properties, an important feature of this new type of model complexes is the rigidity of the dithiolate bridge as well as the orientation of the P=O functionality toward one $Fe(CO)_3$ unit, which is expected to facilitate proton relay from the protonated P=O to the iron site during the catalytic cycle. Furthermore, the electrochemical investigations showed that the reduction of complex **1** is an overall two-electron process with potential inversion. This feature is contrary to the case of $[Fe_2(CO)_5L\{\mu\text{-}(SCH_2)_2NH\}]$ (L = CO, PPh_3, PMe_3)[14a], where these complexes undergo two one-electron reduction steps with the normal ordering of potentials (i.e. $E°_1 - E°_2 > 0$). The potential inversion is a typical result of structural change occurring in the dianionic product, which makes its formation thermodynamically favorable over the monoanion. The structural change, as it has been found by DFT calculations and/or experiments on some [FeFe] models, include: (*i*) elongation of the Fe–Fe bond, (*ii*) cleavage of one of the Fe–S bonds and (*iii*) rotation of one $Fe(CO)_3$ unit to allow orientation of one of its CO ligands into bridging or semi-bridging position to delocalize the negative charge.[17b,28] Increasing the steric bulk at the bridgehead of the model complex decreases the rotational barrier of the $Fe(CO)_3$ units[29] and hence

makes the structural change kinetically more facile. The bulkier bridgehead in complex **1** (i.e. the Ph-P=O group) compared to the N-H in the $[Fe_2(CO)_{6-n}L\{\mu\text{-}(SCH_2)_2NH\}]$ complexes may explain the observed inverted reduction potentials of complex **1**.

In the present work we have explored the influence of substituting one CO in complex **1** by stronger electron donating and more sterically demanding ligands, PPh_3 and $P(OEt)_3$, toward the electrochemical reduction mechanism of the resulting substituted models. We discuss a remarkable difference in the voltammetric behaviour between the PR_3-substituted complexes, which has not been observed before, to the best of our knowledge. Moreover, we have performed DFT calculations to gain insights into the structural changes accompanying the reduction processes of the hexacarbonyl and the substituted complexes.

Results and Discussion

Synthesis. Treatment of an acetonitrile solution of complex **1**[27] with 1 equiv trimethylamine N-oxide ($Me_3NO{\cdot}2H_2O$) at room temperature for 30 min resulted in oxidative abstraction of CO (decarbonylation) to yield the in situ acetonitrile complex (Scheme 1).[30] Subsequent addition of L (PPh_3 or $P(OEt)_3$) afforded the monosubstituted complexes **2** (L = PPh_3) and **3** (L = $P(OEt)_3$) in very high yields (98 %) after stirring for 18 h at room temperature (Scheme 1). No purification was required after removal of the reaction solvent, only filtration.

Scheme 1. Reaction pathway toward monosubstituted complexes **2** and **3**.

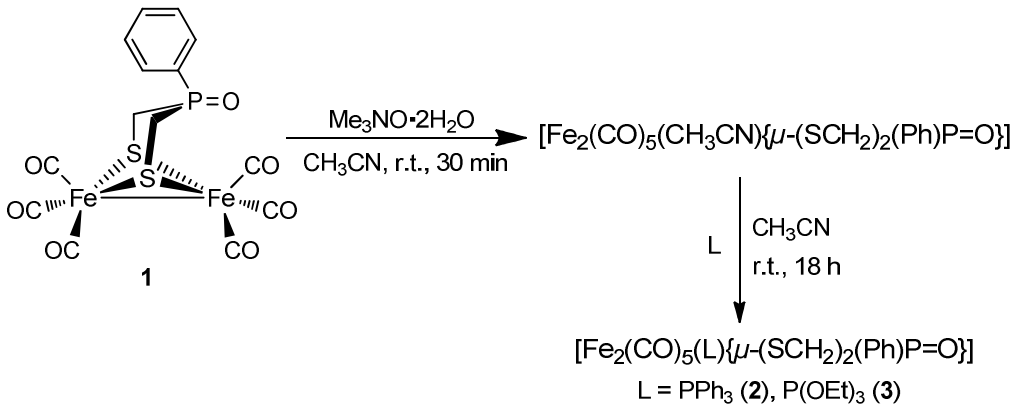

Spectroscopic Characterization. Complexes **2** and **3** were characterized by ^{1}H, ^{13}C and ^{31}P NMR as well as IR techniques, mass spectrometry, elemental analysis and X-ray crystallography. The IR spectrum of complex **2** in CH_2Cl_2 solution exhibits four absorption bands at 1941, 1983, 2002 and 2056 in the carbonyl region. In CH_2Cl_2, the CO ligands of complex **3** stretch at 1946, 1983, 2003 and 2058 cm^{-1}. The carbonyl wavenumbers of complexes **2** and **3** are markedly shifted toward lower values relative to those of the hexacarbonyl complex **1** by 36 and 34 cm^{-1}; respectively, in average. The shift in υ(CO) vibration due to replacement of one CO by PPh_3 is slightly higher than that by $P(OEt)_3$ suggesting that the electron density available for donation to the iron core by PPh_3 is slightly higher than that by $P(OEt)_3$. The ^{1}H NMR spectrum of complex **2** shows a splitting pattern of the methylene protons similar to the case of complex **1**, where the axial and the equatorial protons are diastereotopic. While both proton types are coupled by each other, the H-P geminal coupling is observed only for one proton type. The methylene protons of complex **2** are observed as a doublet at 1.18 ppm ($^{2}J_{HH}$ = 15.20 Hz) and a triplet at 2.32 ppm ($^{2}J_{HH}$ = $^{2}J_{HP}$ = 15.20 Hz). Further signals for the protons of the phenyl groups are detected in the range of 6.8-7.8 ppm. The same splitting pattern is also observed for the dithiolato methylene protons of complex **3**. One proton type resonates at 2.20 ppm as a doublet ($^{2}J_{HH}$ = 14.70 Hz) and the other one at 2.57 ppm as a triplet ($^{2}J_{HH}$ = 14.70 Hz, $^{2}J_{HP}$ = 15.50 Hz). The CH_3 and CH_2 protons of the $P(OEt)_3$ substituent resonate at 1.38 and 4.21 ppm as a triplet and a quintet, respectively. While the splitting pattern of the CH_3 group is a result of coupling with vicinal methylene protons ($^{3}J_{HH}$ = 7.03 Hz), the splitting of the CH_2 arises from H-H and H-P vicinal couplings in equal magnitudes ($^{3}J_{HH}$ = $^{3}J_{HP}$ = 7.03 Hz) leading to the observed quintet. Additional signals in the range of 7.40-7.60 ppm are due to the Ph group of complex **3**. The $^{31}P\{^{1}H\}$ NMR spectrum of complex **2** in CD_2Cl_2 solution exhibits two sharp signals at 34.70 and 65.82 ppm for the P=O and PPh_3, respectively. The $^{31}P\{^{1}H\}$ NMR spectrum of complex **3** in CD_2Cl_2 solution shows one sharp peak at 30.70 ppm for the P=O and a broad one at 170.03 ppm due to the $P(OEt)_3$ substituent. This broadness may arise from the fluxionality of the dithiolate ligand or the $Fe(CO)_2P(OEt)_3$ unit such that the $P(OEt)_3$ ligand exchanges between the apical and the basal sites.[20c,20f,29] Figure S1 displays the $^{31}P\{^{1}H\}$ NMR spectra of complex **3** at variable

temperatures from 20 ºC to -70 ºC) showing that the broad resonance observed at room temperature becomes sharp and a new resonance appears at low temperatures.[20f] The $^{13}C\{^{1}H\}$ NMR spectrum of complex **2** shows a doublet centered at 18.45 ppm due to the methylene carbon atoms ($^{1}J_{CP}$ = 67.60 Hz), signals in the region of 128-136 ppm for the phenyl carbon atoms and two signals at 208.68 and 213.58 ppm for the terminal carbonyl groups of the $Fe(CO)_3$ and $Fe(CO)_2PPh_3$ moieties, respectively. The $^{13}C\{^{1}H\}$ NMR of **3** displays three doublets centered at 16.40 ppm ($^{3}J_{CP}$ = 6.41 Hz), 19.60 ppm ($^{1}J_{CP}$ = 62.09 Hz) and 61.95 ppm ($^{2}J_{CP}$ = 4.58 Hz) assigned to the CH_3 groups of the $P(OEt)_3$ substituent, the methylene carbon atoms of the dithiolato bridge, and the methylene carbon atoms of $P(OEt)_3$, respectively. The signals observed in the region of 128-135 ppm are due to the aromatic carbon atoms. The singlet at 208.84 ppm and the doublet centered at 212.33 ppm ($^{2}J_{CP}$ = 16.30 Hz) are attributed to CO groups in the $Fe(CO)_3$ and $Fe(CO)_2P(OEt)_3$ moieties, respectively.

Regioselectivity of Substitution. Indeed, the $^{31}P\{^{1}H\}$ and $^{13}C\{^{1}H\}$ NMR spectroscopic data describe the regioselectivity of the substitution reactions on complex **1** to afford complexes **2** and **3**. The $^{13}C\{^{1}H\}$ NMR spectrum of complex **1** at room temperature, which exhibits two resonance signals at 205.99 and 207.04 ppm,[27] is consistent with nonequivalent $Fe(CO)_3$ units as a consequence of a desymmetrizing effect of the dithiolate linker, μ-$(SCH_2)_2PhP{=}O$. In principle, there are two possible regioisomers resulting from the substitution of one CO in **1** by a PR_3 ligand: a regioisomer with PR_3 located under the P=O functionality and another one having PR_3 under the Ph group, respectively. The $Fe(CO)_3$ and $Fe(CO)_2PPh_3$ moieties of these two possible regioisomers should be nonequivalent. Nevertheless, the $^{31}P\{^{1}H\}$ NMR spectrum of **2** or **3** is consistent with the presence of only a single regioisomer (65.82 or 170.0 ppm for the PPh_3 or $P(OEt)_3$, respectively). Moreover, $^{13}C\{^{1}H\}$ NMR spectra confirm the presence of only one type of $Fe(CO)_3$ and $Fe(CO)_2PR_3$ moieties in **2** and **3**, consistent with only one regioisomer for each monosubstituted complex. The regiochemistry of substitution of one CO ligand in $[Fe_2(CO)_6\{\mu$-$(SCHMe)_2NH\}]$ by PMe_3 or PPh_3 was described by Rauchfuss and co-workers.[25]

Molecular Structures. Single crystals suitable for X-ray diffraction studies were obtained by diffusion of pentane into a CH_2Cl_2 solution of complex **2** at 4 ºC and by evaporation of CH_2Cl_2 solution

of complex **3** at 4 ºC overnight. The molecular structures and the numbering schemes of the complexes are shown in Figure 2. The crystal of complex **2** contains three independent molecules, only one of which is shown in Figure 2.

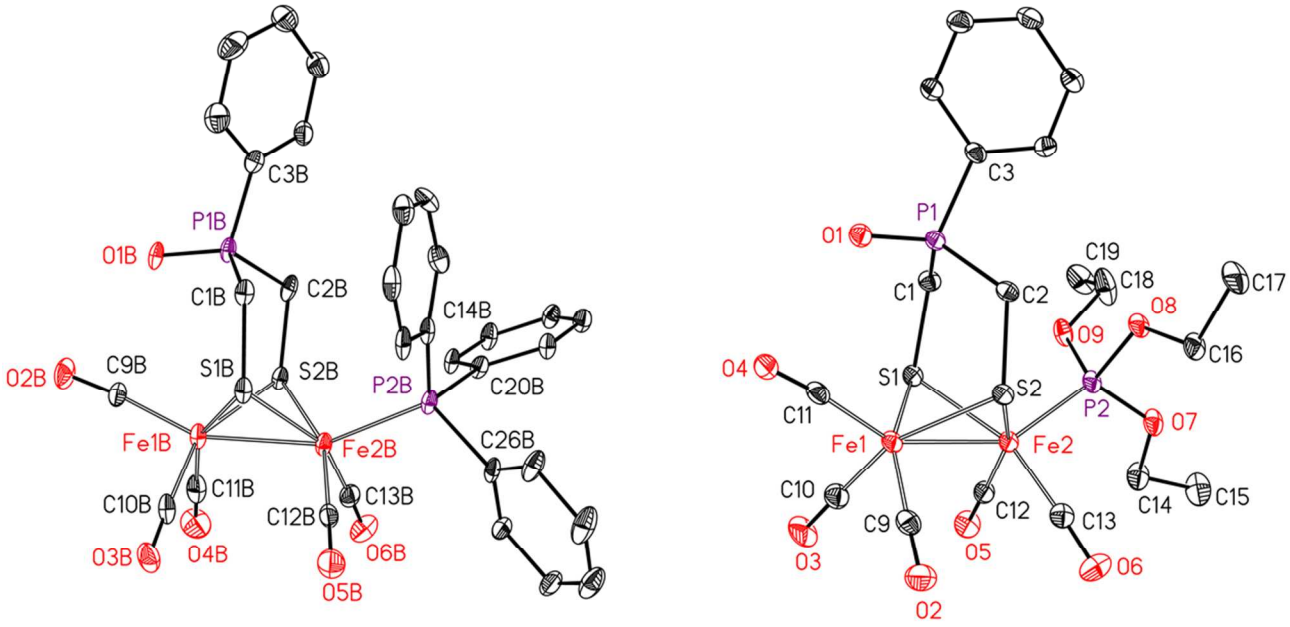

Figure 2. ORTEP view (40 % probability level) of complexes **2** (to the left) and **3** (to the right). Selected bond lengths [Å] and angles [º] of **2** (average): Fe1-Fe2 2.5006(14), Fe2-P2 2.233(2), C9-Fe1-Fe2 156.4(3), P2-Fe2-Fe1 155.4(8). For complex **3**: Fe1-Fe2 2.5152(8), Fe2-P2 2.1687(12), C11-Fe1-Fe2 151.57(13), P2-Fe2-Fe1 147.93(4).

As it can be seen from Figure 2, each iron core in complexes **2** and **3** adopts a distorted octahedral structure. In both complexes the two iron atoms are bridged by the dithiolate linker $(SCH_2)_2(Ph)P{=}O$, the CO ligands at the Fe1 sites are facial and the PR_3 ligands coordinate to the Fe2 sites on apical position. The bicyclic $[Fe_2S_2]$ structure in these complexes reveals a butterfly conformation. The phosphorus atom of the dithiolate bridge is surrounded in a distorted tetrahedral fashion. Indeed, the molecular structures (Figure 2) identify the regioselectivity of the substitution reactions where the PR_3 ligands are located away from the oxygen atom of the P=O functionalities of complexes **2** and **3**. While the PR_3 ligands of complexes **2** and **3** are on the apical positions of the iron atoms, the situation can be different in solution due to the apical/basal site exchange of the ligands at the $Fe(CO)_2PR_3$ units.[20c,20f,29]

In both complexes, the P=O functionalities are oriented toward the Fe1 atom making them potential proton relay models.

The Fe-Fe bond lengths in complexes **2** and **3** (2.5006(14) Å (average) and 2.5152(8) Å, respectively) are comparable to each other and to that in complex **1** (2.5148(9) Å)[27], but slightly shorter than those of the H cluster (2.55-2.62 Å)[7,8,11a]. The average Fe2-P2 bond length in complex **2** is 2.233(2) Å, which is longer than the Fe2-P2 bond length in complex **3** (2.1687(12) Å). These values are consistent with the average Fe-PPh_3 and Fe-$P(OEt)_3$ bond lengths (2.247 Å and 2.1808 Å, respectively) in various [FeFe]-hydrogenase complexes.[18b,20a,31] The difference of 0.06 Å between the Fe-PPh_3 and Fe-$P(OEt)_3$ bond lengths can be attributed mainly to the higher π-acidity of $P(OEt)_3$ compared to that of PPh_3.[32]

In Figure 3, we show the effect of the bulkiness of the Ph-P=O moiety as well as the PR_3 ligand in complexes **2** and **3** on the angles OC^{ap}-Fe1-Fe2 (the superscript ap for apical) and R_3P-Fe2-Fe1. We compare the angles with those in complex **1** as well as the previously reported complex **4**, $[Fe_2(CO)_6\{\mu\text{-}(SCH_2)_2CH_2\}]$[33]. We can notice that the angle OC^{ap}-Fe1-Fe2 is the smallest in complex **4** (148.32º) compared to those of the other complexes that have bulkier μ-$(SCH_2)_2PhP{=}O$ moieties than μ-$(SCH_2)_2CH_2$ in complex **4**. The angle OC^{ap}-Fe2-Fe1, 146.12(16)º, in complex **1** is smaller than that of OC^{ap}-Fe1-Fe2, 152.17(14)º, owing to the steric interaction between the P=O functionality and the apical CO coordinated to Fe1. The angles OC^{ap}-Fe2-Fe1 in complex **1**, 146.12(16)º, and OC^{ap}-Fe1-Fe2, 148.32º, in complex **4** are comparable, which implies that the spatial region between the Ph ring at the bridgehead of complex **1** and the apical CO at Fe2 has minimum steric interaction. Even when one CO in complex **1** is substituted by $P(OEt)_3$, there is still no significant steric interaction between the apical ligand at Fe2 and the Ph group as indicated by the comparable OC^{ap}-Fe2-Fe1 (146.12(16)º) and $(EtO)_3P$-Fe2-Fe1 (147.93(4)º) angles in complexes **1** and **3**, respectively. However, the distortion in angles becomes clearer in the case of complex **2** compared to the others. The Ph_3P-Fe2-Fe1 angle (155.38(8)º in average) is larger than the $(EtO)_3P$-Fe2-Fe1 angle because the cone angle of PPh_3 (145°)[34] is significantly larger than that of $P(OEt)_3$ (109°)[34]. This steric interaction between the bulky

PPh_3 and the Ph group results in an increased OC^{ap}-Fe1-Fe2 angle (156.4(3)º in average) compared to those in complexes **1** and **3** (152.17(14)º and 151.57(13)º, respectively).

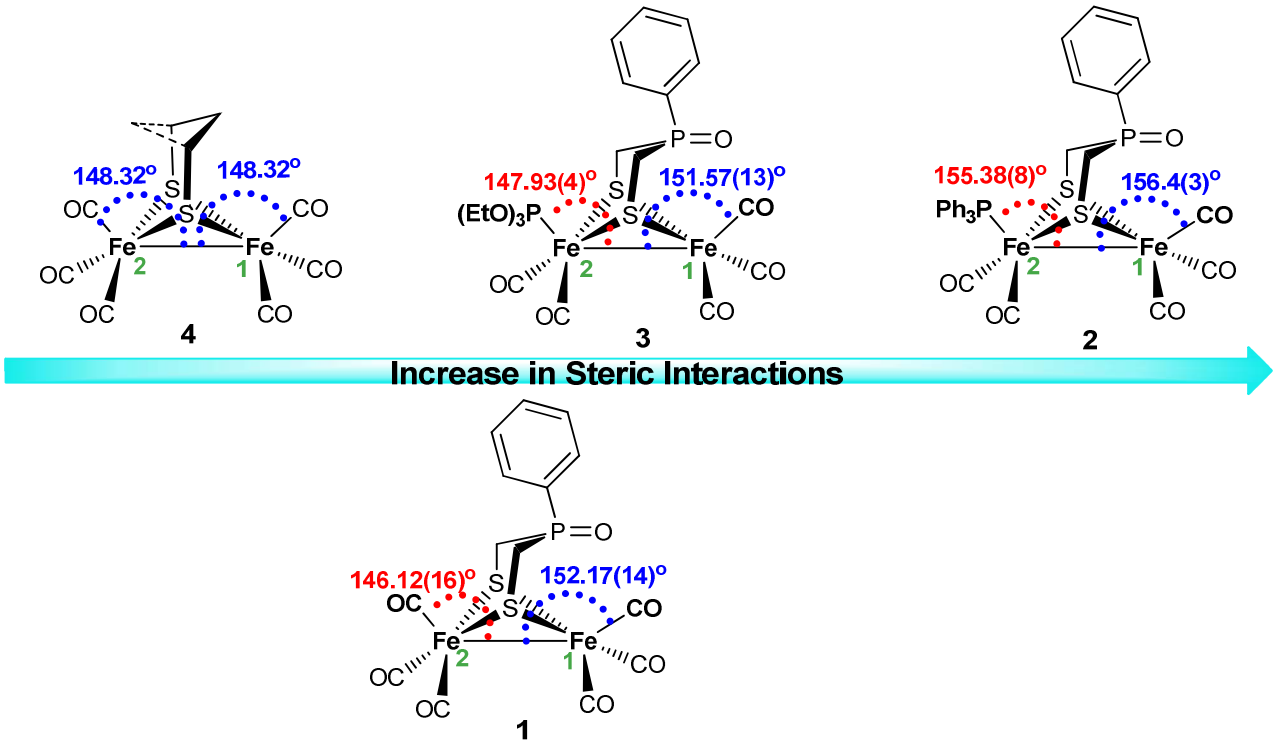

Figure 3. Comparison of selected bond angles [º] in complexes **1**-**4**.

Electrochemistry. Complex **1** is already known to undergo a quasi-reversible two-electron reduction in CH_3CN/NBu_4PF_6 solution at $E_{1/2}$ = -1.34 V (E_{pc} = -1.39 V and E_{pa} = -1.30 V at 0.2 $V{\cdot}s^{-1}$) using mercury drop electrode.[27] In CH_2Cl_2/NBu_4PF_6 solution, complex **1** also exhibits a quasi-reversible two-electron redox couple but at $E_{1/2}$ = -1.48 V (E_{pc} = -1.52 V and E_{pa} = -1.43 V at 0.2 $V{\cdot}s^{-1}$) using a glassy carbon electrode. The electrochemical behavior of complex **1** in CH_2Cl_2/NBu_4PF_6 solution at different scan rates is shown in Figure S2. The plots of the cathodic current (I_p^c) versus the square root of scan rate ($v^{½}$) are linear (Figures S3). Indeed, performing the cyclic voltammetry of $O{=}P(Ph)(CH_2Cl)_2$ in CH_2Cl_2/NBu_4PF_6 solution (Figure S4) showed that the phosphine oxide functionality is not reduced and hence it does not lead to interferences in the measurements of the reduction of this class of [FeFe]-hydrogenase models. To investigate the influence of substituting one CO ligand in complex **1** by PPh_3 and $P(OEt)_3$ toward the redox properties of the iron complexes, cyclic voltammetric studies on complexes **2** and **3** have been performed in CH_2Cl_2 using a glassy carbon working electrode.

The cathodic process of complexes **2** and **3** is closer to an overall two-electron reduction, which occurs at potentials of E_{pc} = -1.78 V and -1.75 V, respectively. The two-electron assignment is based on comparing the normalized cathodic peak current (I_p^c/c; c = concentration of complex) of complexes **2** and **3** with that of complex **1** as well as with the first reduction wave in the cyclic voltammogram of $[Fe_2(CO)_6\{\mu\text{-}Cl_4bpdt\}]$[35] (bpdt = biphenyl-2,2′-dithiolate) under similar conditions. The complex $[Fe_2(CO)_6\{\mu\text{-}Cl_4bpdt\}]$ is already known to exhibit two well-resolved reversible one-electron reduction waves. We have performed DFT calculations to study the structural changes during the reduction of complexes **1**, **2** and **3** (see later). The reduction potential of complex **2** is slightly more negative than that of complex **3** suggesting that PPh_3 is a slightly better donor than $P(OEt)_3$, which is in agreement with the ligand electrochemical parameters (E_L) determined by Lever[36] for $P(OMe)_3$ (E_L = 0.42 V) and PPh_3 (E_L = 0.39). Unexpectedly, the reduction of complex **3** is much more reversible chemically than that of complex **2**. Thus, while complex **3** undergoes a quasi-reversible reduction at slow to moderate scan rates (0.1-2 $V{\cdot}s^{-1}$; Figure 4a), the reversibility of the reduction of complex **2** appears to be much more scan rate dependent (Figure 4b). The reduction of complex **2** is totally irreversible at 0.05 $V{\cdot}s^{-1}$ and only a very small re-oxidation peak can be detected at ~ -1.65 V on the return scan upon increasing the scan rate. An additional oxidation feature can be seen in Figure 4b at E_{pa} = -1.42 V when the scan rate is 0.2 $V{\cdot}s^{-1}$, a potential that was reported for the oxidation of the hexacarbonyl complex **1** at the Fe^0Fe^0 redox state. This may suggest at this stage of the discussion that the reduction of complex **2** induces the formation of $\mathbf{1}^{2-}$ through the displacement of the PPh_3 ligand in $\mathbf{2}^-$ and/or $\mathbf{2}^{2-}$ by a CO ligand coming from another carbonylated species, **S(CO)**, during the reductive process. The enhancement of the chemical reversibility of the two-electron reduction of complex **2** becomes clearer at higher scan rates (Figure S5). We may explain the enhanced reversibility of the redox couple (Fe^IFe^I/Fe^0Fe^0) of complex **2** at the higher scan rates in terms of the shorter reaction time scale for the conversion of $\mathbf{2}^-$ and $\mathbf{2}^{2-}$ into $\mathbf{1}^-$ and $\mathbf{1}^{2-}$, respectively.

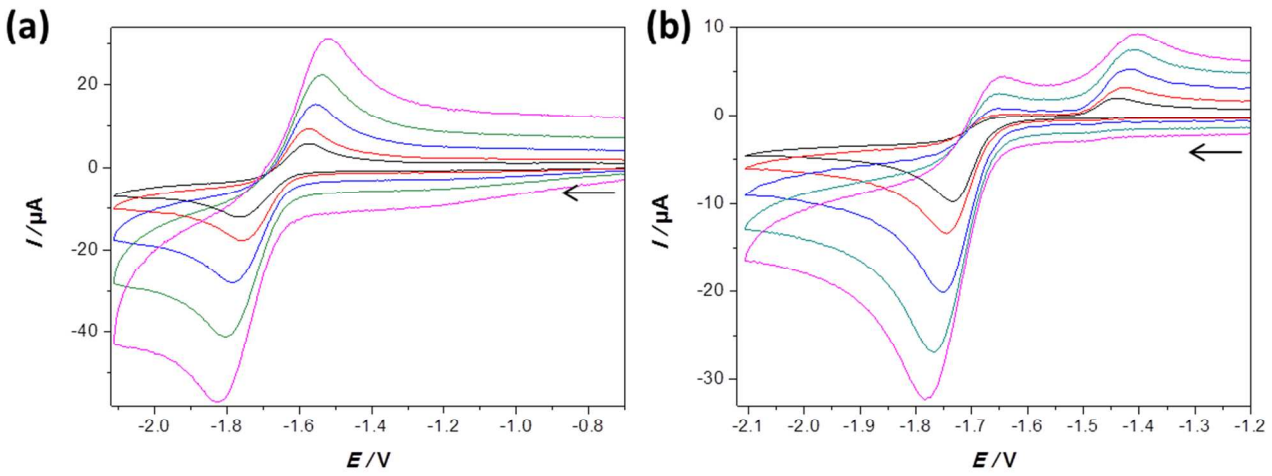

Figure 4. Cyclic voltammetry (CH_2Cl_2/NBu_4PF_6 solution) of (a) 0.51 mM $[Fe_2(CO)_5(P(OEt)_3)\{\mu\text{-}(SCH_2)_2(Ph)P{=}O\}]$ (**3**) at scan rates ($V{\cdot}s^{-1}$) = 0.1 (black), 0.2 (red), 0.5 (blue), 1 (green) and 2 (purple) and (b) 0.408 mM $[Fe_2(CO)_5(PPh_3)\{\mu\text{-}(SCH_2)_2(Ph)P{=}O\}]$ (**2**) at scan rate ($V{\cdot}s^{-1}$) = 0.05 (black), 0.1 (red), 0.2 (blue), 0.4 (green) and 0.6 (purple). *E* is in V against the ferrocenium/ferrocene couple. The arrows indicate the scan direction.

The oxidation wave at -1.42 V (Figure 4b) is found to be reversible on the second cycle as a new reduction event at E_{pc} = -1.52 V is observed and assigned to the process **1** + $2e^-$ → $\mathbf{1}^{2-}$ (Figure 5, the black curve). The current of the anodic and the cathodic peaks of the $\mathbf{1}/\mathbf{1}^{2-}$ couple are increased when the electrochemical measurements are performed using CO-saturated CH_2Cl_2/NBu_4PF_6 solutions (Figure 5, the red curve). These results show that the presence of CO assists the conversion of $\mathbf{2}^-$ or $\mathbf{2}^{2-}$ into $\mathbf{1}^-$ or $\mathbf{1}^{2-}$ at the electrode surface. Our DFT calculations (see later) provided us hints that the loss of PPh_3 is more likely after the first electron reduction of complex **2**. Nonetheless, the possible loss of PPh_3 from $\mathbf{2}^{2-}$ cannot be ruled out. The mechanism that describes the cathodic processes of complex **2** in the absence and presence of CO is shown in Scheme 2.

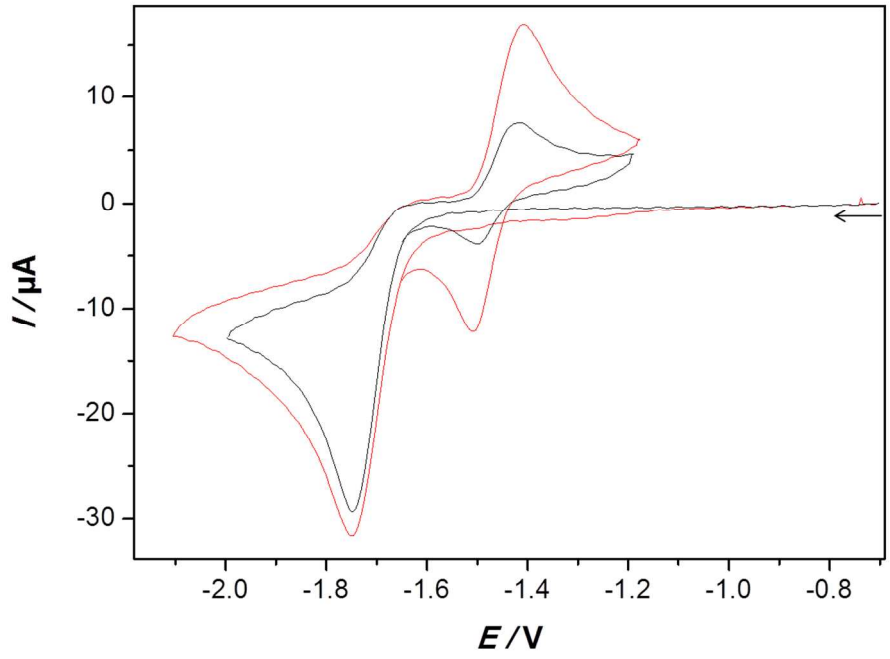

Figure 5. Cyclic voltammograms (CH_2Cl_2/NBu_4PF_6 solution) of 0.558 mM $[Fe_2(CO)_5(PPh_3)\{\mu\text{-}(SCH_2)_2(Ph)P{=}O\}]$ (**2**) at 0.2 $V{\cdot}s^{-1}$ under N_2 (black) and under CO (red). *E* is in V against the ferrocenium/ferrocene couple. The arrow indicates the initial scan direction.

Scheme 2. Proposed reaction scheme for the cathodic processes of complex **2** in the absence or presence of CO (in red). **S(CO)** refers to any species that act as a source of CO when the experiment is done under N_2 atmosphere.

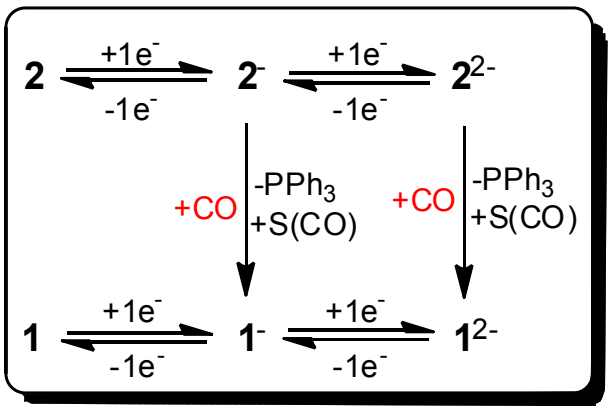

In addition, we have investigated the electrochemical behaviour of complex **3** in CO-saturated CH_2Cl_2/NBu_4PF_6 solution (Figure 6). The current intensity due to the process $\mathbf{3}^{2-} \rightarrow \mathbf{3} + 2e^-$ is visibly

lowered after saturating the solution with CO and a new oxidation event due to a product **P** is detected at $E_{1/2}$ ~ -0.9 V (E_{pa} = -0.843 V, E_{pc} = -0.952 V), which shows reversibility in the reverse scan. Scheme 3 summarizes the reductive processes in the absence and presence of CO. We suggest that **P** might be obtained from the reaction of CO with $\mathbf{3}^{2-}$, an EEC path (E = electron transfer; C = chemical reaction). The fact that P undergoes reversible oxidation indicates that the reaction of $\mathbf{3}^{-}$ with CO to afford an intermediate **{I}** followed by reduction to give **P** is also a possibility; i.e. an ECE path to **P**. Undoubtedly, a mechanism involving displacement of $P(OEt)_3$ by CO at the redox levels Fe^0Fe^I or Fe^0Fe^0 of complex **3** is not operative because the reversible redox couple (Fe^IFe^I/Fe^0Fe^0) of complex **1** was not detected in contrast to the case of complex **2**. Attempts to gain insight into the structure of P have been made by using DFT calculations, which suggest that **P** may retain a bimetallic structure featuring two $[Fe(CO)_4]$ and $\{Fe(CO)_2(P(OEt)_3)[(SCH_2)_2(Ph)P{=}O]\}$ moieties that could be linked through one sulfur atom or a weak iron-iron interaction (Supplementary Material).

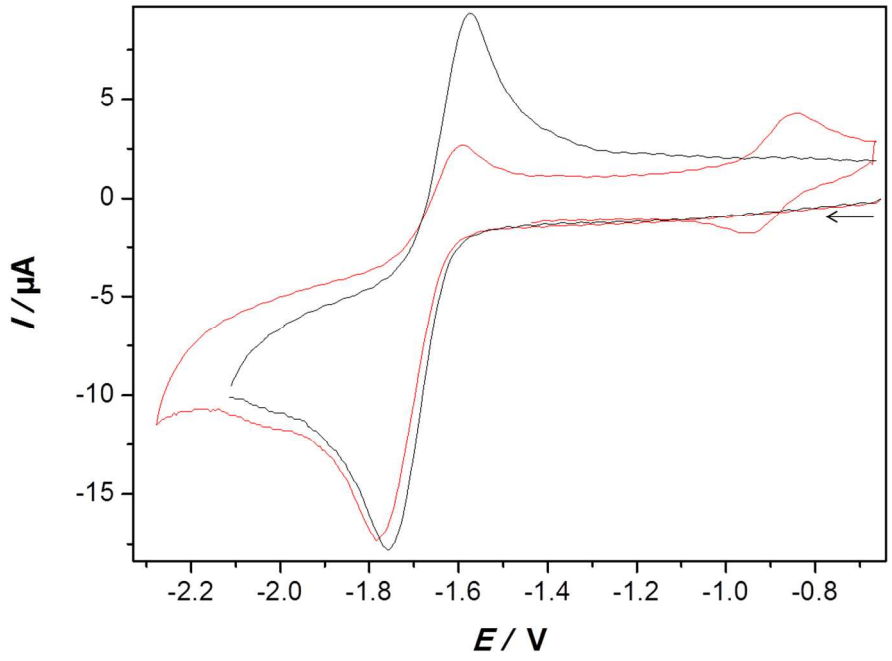

Figure 6. Cyclic voltammetry (CH_2Cl_2/NBu_4PF_6 solution) of 0.51 mM $[Fe_2(CO)_5(P(OEt)_3)\{\mu\text{-}(SCH_2)_2(Ph)P{=}O\}]$ (**3**) at 0.2 $V{\cdot}s^{-1}$ under N_2 (black) and CO (red). *E* is in V against the ferrocenium/ferrocene couple. The arrow indicates the initial scan direction.

Scheme 3. Proposed reaction scheme for the cathodic processes of complex **3** under N_2 (black arrows) and CO (red arrows).

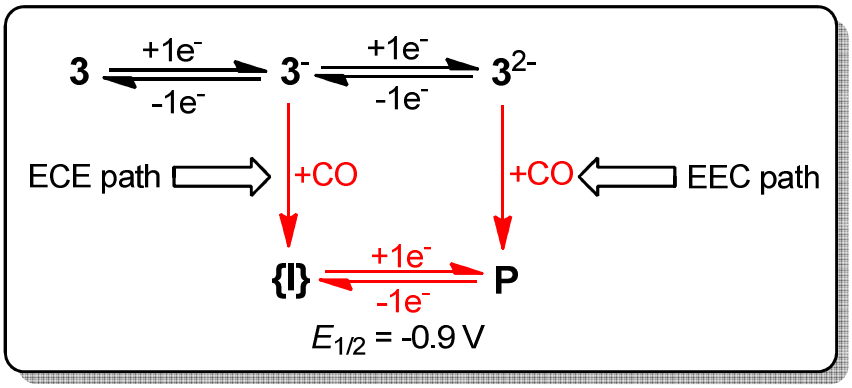

Figure 7 shows that increasing the scan rate results in an increase of the reversibility of the reduction of complex **3** under a CO atmosphere, due to a lower conversion of the reduced species into **P**. The reason for this is, again, that the reaction time becomes too short for the chemical process to take place extensively at faster scan rates.

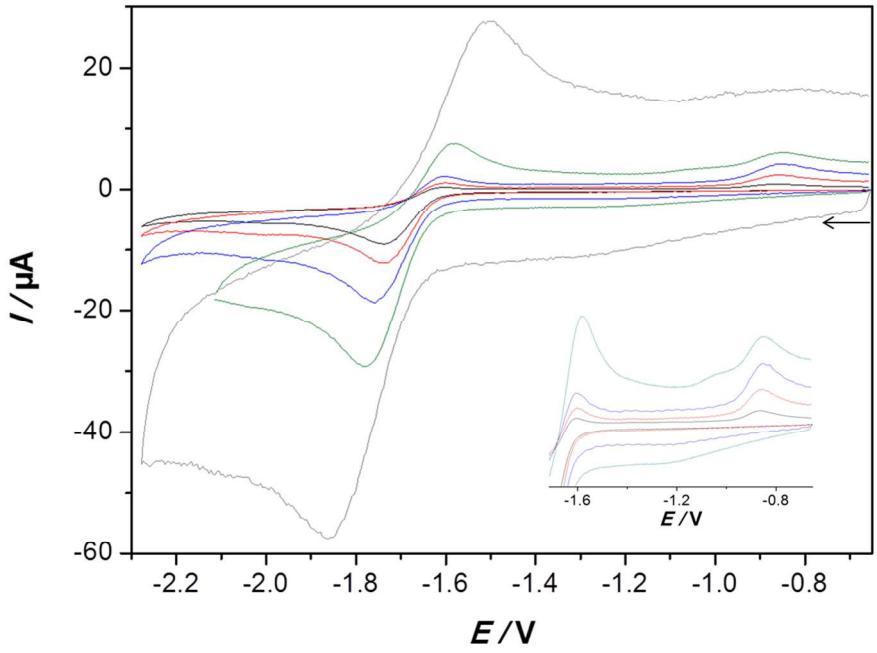

Figure 7. Cyclic voltammetry of 0.51 mM $[Fe_2(CO)_5(P(OEt)_3)\{\mu\text{-}(SCH_2)_2(Ph)P{=}O\}]$ (**3**) in CO-saturated CH_2Cl_2/NBu_4PF_6 solution at scan rates ($V{\cdot}s^{-1}$) = 0.05 (black), 0.1 (red), 0.2 (blue), 0.5 (green) and 2 (grey). The inset shows only the range where the two oxidation peaks occur at the scan rates indicated except the gray curve. *E* is in V against the ferrocenium/ferrocene couple. The arrow indicates the scan direction.

The stability of Fe-PR_3 against dissociation should be related to the factors affecting the strength of the Fe-P bond during the reduction steps. We have discussed before (X-ray structures) that the Fe-P bond length in the *neutral* complex **3** is shorter than that in complex **2** because the π-back donation n{Fe}→σ*{P-O} is in higher extent than n{Fe}→σ*{P-C}, where n refers to the non-bonding electrons of the Fe atoms. This electronic effect may play a role toward the stability against dissociation of the Fe-PR_3 bond. Additionally, it is well known that the rate of dissociation of a metal-ligand bond is accelerated for bulky ligands.[34a,37] We have shown before how PPh_3 has a more pronounced effect on the bond angles of complex **2** than $P(OEt)_3$ does in complex **3** because of the larger cone angle of PPh_3 (145°)[34] compared to $P(OEt)_3$ (109°)[34]. The stepwise electron transfer processes result in structural changes (bond distances, bond angles and stereochemistry) within the $[Fe_2S_2]$ core as it was described for various [FeFe] models.[18a,28,38] To gain insights on these structural changes, we have performed DFT

calculations for the neutral, monoanion and dianion of complexes **1**, **2** and **3**, which might provide hints on the factors governing the stability of the Fe-P bond after each electron transfer step.

DFT calculations.

The structures of the dinuclear iron compounds **1**, **2** and **3** have been calculated using the program package GAUSSIAN09.[39,40] For iron atoms a relativistic ECP of the Stuttgart-Dresden group (SDD) has been applied.[41] Moreover, analogous compounds with L = PMe_3 (**5**) and $P(OMe)_3$ (**6**) have been calculated. The corresponding results may be found as supplementary information (Table S1 and Figure S6 as well as Figure S7). In recent years a number of results of theoretical calculations concerning [FeFe]-hydrogenase models and various aspects of their reactivity and chemical properties as e.g. oxygen affinity, isomerizsation triggered by protonation, electrochemistry or photochemistry have been published.[10b,21b,28b,33,38,42] They clearly show that DFT calculations may be considered a tool to understand the experimentally observed behaviour of such model compounds.

The iron carbonyl compounds **1**-**3**, **5** and **6** have been considered in the neutral state as well as the products of a formal one- and two-electron reduction. In the case of two electron reduction (i.e. formation of a dianion), it turned out that a rearranged geometry in which only one sulfur atom is acting as a bridging ligand is energetically preferred compared to geometries with two bridging sulfur atoms. Scheme 4 summarizes the structural formulae of the species **1**-**3** in the neutral and reduced forms. Figure 8, Figure S8 and Figure S9 show the calculated molecular structures of all compounds mentioned in Scheme 4 together with the DFT total energies (E_T) relative to the neutral species with the same set of ligands, the number of imaginary frequencies for all stationary points calculated and the most important calculated bond lengths.

Scheme 4. Calculated structures of **1-3** in the neutral, monoanionic and dianionic state.

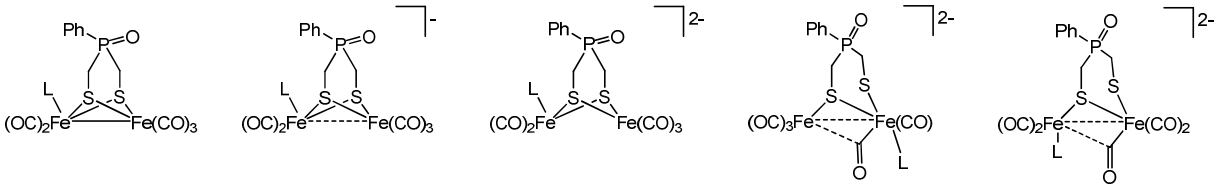

L = CO	**1**	**1**$^{-}$	**1**$^{2-}$	**1a**$^{2-}$	
L = PPh_3	**2**	**2**$^{-}$	**2**$^{2-}$	**2a**$^{2-}$	
L = $P(OEt)_3$	**3**	**3**$^{-}$	**3**$^{2-}$	**3a**$^{2-}$	**3b**$^{2-}$

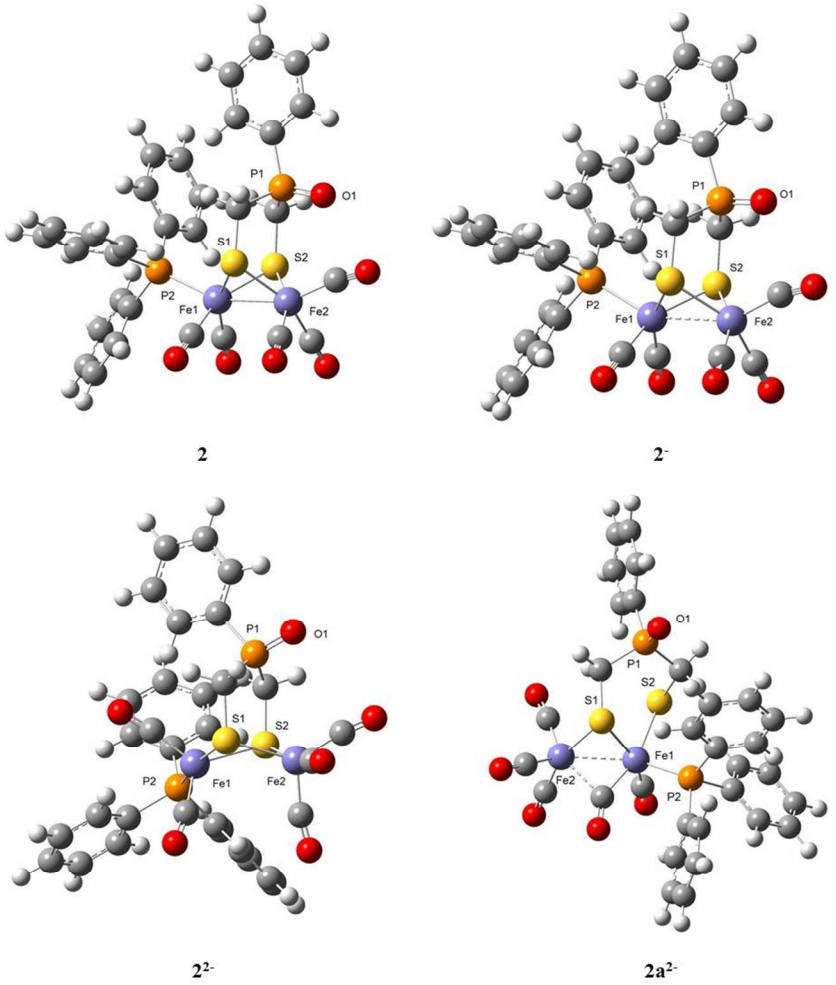

Figure 8. Calculated molecular structures and selected bond lengths [pm] of **2**: HF = -3374.353390 a.u., *NImag* = 0, Fe1-Fe2 251.6, Fe1-S1 234.7, Fe1-S2 235.0, Fe2-S1 233.9, Fe2-S2 233.4, Fe1-P2 231.4, P1-O1 150.0; $\mathbf{2}^-$: HF = -3374.415431 a.u. (-162.9 kJ·mol^{-1} relative to **2**), *NImag* = 0, Fe1-Fe2 274.8, Fe1-S1 238.0, Fe1-S2 238.0, Fe2-S1 240.2, Fe2-S2 238.6, Fe1-P2 241.3, P1-O1 150.2; $\mathbf{2}^{2-}$: HF = -3374.356295 a.u. (-7.6 kJ·mol^{-1} relative to **2**), *NImag* = 0, Fe1-Fe2 350.4, Fe1-S1 237.1, Fe1-S2 245.3, Fe2-S1 242.2, Fe2-S2 240.0, Fe1-P2 222.2, P1-O1 151.2; $\mathbf{2a}^{2-}$: HF = -3374.367309 a.u. (-36.5 kJ·mol^{-1} relative to **2**), *NImag* = 0, Fe1-Fe2 261.0, Fe1-S1 237.4, Fe1-S2 250.4, Fe2-S1 236.3, Fe1-P2 224.0, P1-O1 151.6.

The results depicted in Figure 8, Figure S8 and Figure S9 show some interesting trends concerning the relative energies of the compounds although it has to be kept in mind that these calculations are gas phase calculations. So differences in the energies of compounds in different oxidation states do not allow an estimate of real redox potentials or whether a one-electron reduction is preferred over a two-electron process. According to our calculations the product of the one-electron reduction ($\mathbf{1}^-$, $\mathbf{2}^-$, $\mathbf{3}^-$) is always the thermodynamically most stable compound as it is expected due to the typically observed negative electron affinity for the first reduction step whereas the second reduction normally is hampered for electrostatic reasons. In the dianionic state, there are two possible structural arrangements. Either the $[Fe_2S_2]$ core remains a symmetrical building block with two bridging thiolate functions ($\mathbf{1}^{2-}$, $\mathbf{2}^{2-}$, $\mathbf{3}^{2-}$ in Scheme 4) or there is a rearrangement leading to an unsymmetrical coordination mode with one bridging thiolate and one thiolate that binds only to one of the iron atoms. In the latter case there are of course two isomers if L ≠ CO with the ligand being bonded to the iron atom exhibiting two Fe-S bonds ($\mathbf{2a}^{2-}$, $\mathbf{3a}^{2-}$) or the ligand is coordinated to the iron atom with only one additional iron sulfur bond ($\mathbf{3b}^{2-}$). For all ligands L = CO, PPh_3 and $P(OEt)_3$ the rearranged cluster compounds are thermodynamically favored with respect to the isomers showing a symmetrical $[Fe_2S_2]$ cluster core. In addition, the compounds with L ≠ CO show an enhanced stability for the dianionic isomers with the ligand being bonded to the iron showing two iron-sulfur contacts. The same trends are observed for derivatives with L = PMe_3 and $P(OMe)_3$ (*cf.* Supplementary Material).

The calculated bond lengths (Figure 8, Figure S8 and Figure S9) show that upon subsequent reduction of **1**, **2** or **3**, the Fe-Fe distance significantly increases. Correspondingly, the butterfly structure of the $[Fe_2S_2]$ core in the neutral species gets flattened upon reduction ending up to be a bended four-membered ring system in $\mathbf{1}^{2-}$, $\mathbf{2}^{2-}$ and $\mathbf{3}^{2-}$. In the dianionic compounds with a rearranged coordination sphere around the iron atoms ($\mathbf{1a}^{2-}$, $\mathbf{2a}^{2-}$, $\mathbf{3a}^{2-}$ and $\mathbf{3b}^{2-}$), one Fe-S bond is cleaved with respect to the symmetric isomers $\mathbf{1}^{2-}$, $\mathbf{2}^{2-}$ and $\mathbf{3}^{2-}$. The Fe-S bond cleavage leads to quite short iron-iron interaction to compensate the electron deficient situation of the iron atom that shows only one Fe-S coordination. This

is also the reason for the observation of one semi-bridging CO ligand in **1a**$^{2-}$, **2a**$^{2-}$ and **3b**$^{2-}$. Interestingly, this interaction is not observed for **3a**$^{2-}$ (and **6a**$^{2-}$, cf. Supplementary Material).

It has been shown by the CV measurements that upon reduction of **2**, a significant amount of the hexacarbonyl cluster **1** is formed owing to the loss of PPh_3 and subsequent CO addition. Nevertheless, it is not clear whether the elimination of CO takes place after the first or after the second reduction step. Bond length data demonstrate that the first reduction step induces an elongation of the iron phosphorous bond in **2**$^{-}$ compared to **2**, whereas the corresponding bond is quite short in both isomeric compounds **2**$^{2-}$ and **2a**$^{2-}$ after the second reduction step. We therefore estimated the structural implications of the loss of PPh_3 from both **2**$^{-}$ and **2a**$^{2-}$ and subsequent addition of CO to the calculated intermediates.

If PPh_3 is eliminated from **2**$^{-}$ the resulting anion **7** (Figure 9) shows almost identical structural features of the remaining molecule compared to **2**$^{-}$. The $[Fe_2S_2]$ core is still highly symmetrical although Fe-S and Fe-Fe bond lengths are shortened with respect to **2**$^{-}$ in order to compensate the loss of two electrons. A monoanionic isomer with a rearranged cluster core as in the doubly reduced species **2a**$^{2-}$ is no minimum on the hyper surface of the monoanion even after PPh_3 is eliminated. If, on the other hand, PPh_3 is split off from the dianion **2a**$^{2-}$ the unsymmetrical coordination mode is retained to produce the dianionic intermediate **8**. In contrast to the starting compound (**2a**$^{2-}$), all CO ligands in **8** are now coordinated in a terminal fashion and the Fe-S and Fe-Fe bonds are also shortened as it has been observed in **7**. Interestingly, an isomeric starting compound with three CO ligands coordinated to the iron atom with two iron sulfur contacts and only two CO ligands at the other metal upon geometry optimization ends up in the geometry of **8** since during the calculations one CO is shifted from one iron to the other. From this data it cannot be judged whether the substitution of PPh_3 against CO proceeds from the monoanionic and the dianionic state although the highly elongated iron phosphorous bond length in **2**$^{-}$ may give a hint that elimination of PPh_3 from this substrate might be the more likely reaction pathway. The higher Fe-P elongation in case of Fe-PPh_3 bond (9.9 pm) compared to that of Fe-$P(OEt)_3$ (1.1 pm) upon first electron reduction is attributed to the weaker π-acidity of PPh_3 compared to $P(OEt)_3$ as well as the higher steric clash between PPh_3 and the PhP=O group. In the dianion **2a**$^{2-}$, the

Fe-PPh_3 bond length is even shorter than in the neutral **2** (Figure 9). This shortening could be due to steric and electronic reasons such that the rearrangement minimizes the steric interaction between PPh_3 and the PhP=O group and lowers the electron density at the [FeFe] core via Fe-S bond cleavage and forming μ-CO. Thus, for these electronic and steric reasons we suggest that the dissociation of the Fe-PPh_3 bond is likely to occur at the monoanionic state before the rearrangement process on the dianion.

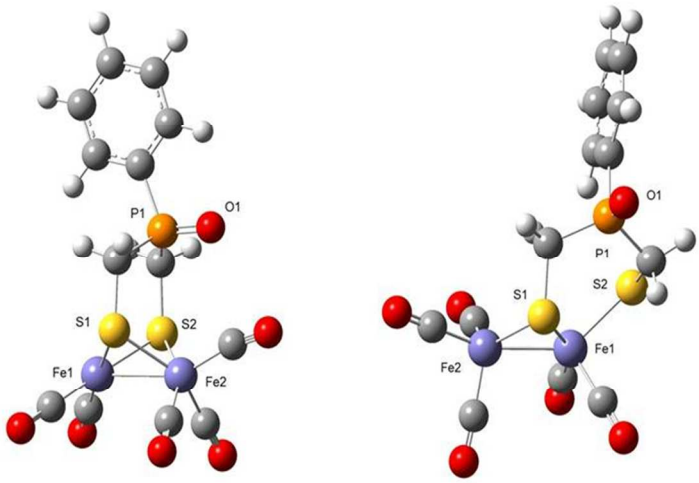

Figure 9. Calculated molecular structures and selected bond lengths [pm] of **7**: HF = -2338.194025 a.u., *NImag* = 1 (the very weak imaginary frequency corresponds to the rotation of the iron carbonyl groups relative to each other), Fe1-Fe2 260.8, Fe1-S1 233.6, Fe1-S2 233.6, Fe2-S1 239.4, Fe2-S2 239.4, P1-O1 150.1; **8**: HF = -2338.153575 a.u., *NImag* = 0, Fe1-Fe2 243.7, Fe1-S1 229.5, Fe1-S2 232.7, Fe2-S1 232.3, P1-O1 151.7.

Conclusions

The monosubstitution of CO ligand in complex **1** by PPh_3 or $P(OEt)_3$ gave complexes **2** and **3**, respectively, in high yields (98 %). The $^{31}P\{^1H\}$ and $^{13}C\{^1H\}$ spectra of complexes **2** and **3** suggest a regioselective substitution of CO by PR_3, which occurs at Fe2 rather than at Fe1 as evident by the molecular structures (Figure 2). X-ray crystallography shows that in both **2** and **3** the PR_3 ligand coordinates at the apical position of the iron atom Fe2 (Figure 2). The $Fe(CO)_3$ units in complexes **1**, **2**

and **3** are more encumbered than the $Fe(CO)_3$ in complex **4**, as evident by comparing their CO^{ap}-Fe1-Fe2 angles, reflecting the steric bulk of the Ph-P=O bridgehead (Figure 3). The angles L^{ap}-Fe2-Fe1 (L = CO, PPh_3, $P(OEt)_3$) are comparable for complexes **1** and **3**, but the largest for complex **2** due to the steric effect of the PPh_3 ligand. Our study finds that the higher steric effect of PPh_3 compared to $P(OEt)_3$ results in remarkable differences in the electrochemical behavior between complexes **2** and **3**. The PPh_3 ligand in complex **2** tends to be released after reduction whereas $P(OEt)_3$ in complex **3** does not. Owing to the lower π-acidity and the larger cone angle of PPh_3 compared to $P(OEt)_3$ and based on the results of the DFT calculations, we suggest that the PPh_3 loss occurs most probably upon the first electron reduction step. The presence of CO in the solution assists the formation of **1** in the cyclic voltammetry of **2** by compensating the loss of PPh_3 from the reduced species of **2**. Cyclic voltammetry of complex **3** shows that the Fe-$P(OEt)_3$ bond is stable against dissociation during the cathodic process at all scan rates and even when the solution is saturated with CO. The presence of CO does not lead to substitute the $P(OEt)_3$ to give the hexacarbonyl, but instead it reacts with the reduced species forming a spectroscopically uncharacterized product **P** (Supporting Information). This work shows how the steric and electronic factors affect the kinetic stability of M-L bonds (M = metal; L = ligand).

Experimental Section

Materials and Techniques.

All reactions were performed using standard Schlenk and vacuum-line techniques under an inert gas (argon or nitrogen). The ^{1}H, $^{1}H\{^{31}P\}$, $^{13}C\{^{1}H\}$, and $^{31}P\{^{1}H\}$ spectra were recorded with a Bruker Avance 200 MHz spectrometer. Chemical shifts are given in parts per million with reference to internal $SiMe_4$ or $CHCl_3$. External standard 85 % H_3PO_4 was used as a reference for $^{31}P\{^{1}H\}$ spectral measurements. The mass spectrum was recorded with a Finnigan MAT SSQ 710 instrument. The IR spectra were measured with a Perkin–Elmer System 2000 FT-IR spectrometer. Elemental analysis was performed with a Leco CHNS-932 apparatus. TLC was performed by using Merck TLC aluminum sheets (Silica gel 60 F254). Solvents from Fisher Scientific and other chemicals from Acros were used

without further purification. All solvents were dried and distilled prior to use according to standard methods. Complex **1** has been prepared according to our reported method.[27]

Theoretical Calculations.

All calculations have been performed on the B3LYP/6-311++g(d,p) level of theory using the program package GAUSSIAN09.[39,40] In addition, frequency calculations have been performed to show that the structures are minima on the hyper surface. For iron atoms we used a relativistic ECP of the Stuttgart-Dresden group (SDD) replacing the 28 core electrons in transition-metal atoms by an effective core potential (ECP) and contracting valence basis sets (8s7p6d) primitive sets to (6s5p3d).[41]

Electrochemistry.

Instrumentation and Procedures.

These experiments do not involve corrections for the *iR* drop. Cyclic voltammetric experiments were performed in a three electrodes cell using a Radiometer potentiostat (μ-Autolab Type-III or an Autolab PGSTAT 12) driven by the GPES software. The working electrode consisted of a vitreous carbon disk (d = 3 mm) that was polished on a felt tissue with alumina before each CV scan. The Ag/Ag^+ reference electrode was separated from the analyte by a CH_2Cl_2-$[NBu_4][PF_6]$ bridge. All the potentials are quoted against the ferrocene-ferrocenium couple; ferrocene was added as an internal standard at the end of the experiments.

Crystal Structure Determination.

The intensity data were collected on a Nonius KappaCCD diffractometer, using graphite-monochromated Mo-K_α radiation. Data were corrected for Lorentz and polarization effects; absorption was taken into account on a semi-empirical basis using multiple-scans.[43-45]

The structure was solved by direct methods (SHELXS[46]) and refined by full-matrix least squares techniques against Fo^2 (SHELXL-97[46]). All hydrogen atom positions were included at calculated

positions with fixed thermal parameters. XP (SIEMENS Analytical X-ray Instruments, Inc.) was used for structure representations.

Crystal Data for complex **2**. $C_{31}H_{24}Fe_2O_6P_2S_2 \cdot CH_2Cl_2$, Mr = 815.19 g·mol^{-1}, brown prism, size 0.052 x 0.048 x 0.034 mm^3, monoclinic, space group C 2/c, a = 68.8713(17), b = 13.5987(4), c = 22.0300(6) Å, β = 100.563(1)°, V = 20282.8(10) Å^3, T = 20 °C, Z = 24, $\rho_{calcd.}$ = 1.602 g·cm^{-3}, μ (Mo-K$_\alpha$) = 12.78 cm^{-1}, multi-scan, transmin: 0.5438, transmax: 0.7890, F(000) = 9936, 49941 reflections in h(-80/80), k(-14/15), l(-25/25), measured in the range 1.76° ≤ Θ ≤ 24.71°, completeness Θmax = 99 %, 17115 independent reflections, R_{int} = 0.0540, 13772 reflections with $F_o > 4\sigma(F_o)$, 1246 parameters, 0 restraints, $R1_{obs}$ = 0.0990, wR^2_{obs} = 0.2294, $R1_{all}$ = 0.1202, wR^2_{all} = 0.2429, GOOF = 1.143, largest difference peak and hole: 2.910 / -1.703 e Å^{-3}.

Crystal Data for complex **3**. $C_{19}H_{24}Fe_2O_9P_2S_2$, Mr = 634.14 g·mol^{-1}, brown prism, size 0.046 x 0.045 x 0.034 mm^3, triclinic, space group P ī, a = 7.6319(5), b = 11.2407(7), c = 16.2017(11) Å, α = 86.524(4), β = 83.504(3), γ = 70.792(3)°, V = 1303.70(15) Å^3, T = -140 °C, Z = 2, $\rho_{calcd.}$ = 1.615 g·cm^{-3}, μ (Mo-K$_\alpha$) = 14.41 cm^{-1}, multi-scan, transmin: 0.4880, transmax: 0.7455, F(000) = 648, 12987 reflections in h(-9/9), k(-14/11), l(-20/19), measured in the range 2.84° ≤ Θ ≤ 26.73°, completeness Θmax = 98.7 %, 5890 independent reflections, R_{int} = 0.0612, 4927 reflections with $F_o > 4\sigma(F_o)$, 310 parameters, 0 restraints, $R1_{obs}$ = 0.0696, wR^2_{obs} = 0.1731, $R1_{all}$ = 0.0809, wR^2_{all} = 0.1857, GOOF = 1.076, largest difference peak and hole: 1.414 / -1.665 e Å^{-3}.

General procedure for synthesis of complexes 2 and 3.

To solution of complex **1** in CH_3CN (20 ml), 1 equiv $Me_3NO \cdot 2H_2O$ was added to give the respective nitrile complex within 30 min, visible by darkening of the red solution. Subsequently, 1 equiv PR_3 was added, and the reaction mixture was stirred at room temperature for 18 h. The resulting red solution was then filtered and the solvent was evaporated using vacuum transfer line to give the complexes in 98% yield.

Complex 2. Complex **1** (46 mg, 0.093 mmol) was treated with $Me_3NO{\cdot}2H_2O$ (10 mg, 0.09 mmol) and PPh_3 (24 mg, 0.092 mmol) according to the general method. $C_{31}H_{24}Fe_2O_6P_2S_2{\cdot}0.5CH_2Cl_2$: C, 48.96; H, 3.26; S, 8.30. Found: C, 49.22; H, 3.27; S, 8.48. Micro-ESI-MS (*m*/*z*): 752.7 $[M + Na]^+$. DEI-MS (*m*/*z*): 674 $[M - 2CO]^+$, 618 $[M - 4CO]^+$, 590 $[M - 5CO]^+$, 440 $[M - CO - PPh_3]^+$, 412 $[M - 2CO - PPh_3]^+$, 384 $[M - 3CO - PPh_3]^+$, 356 $[M - 4CO - PPh_3]^+$ and 328 $[M - 5CO - PPh_3]^+$. IR (CH_2Cl_2): 1941, 1983, 2002, 2056 cm^{-1}. $^{31}P\{^1H\}$ NMR (200 MHz, CD_2Cl_2): δ 30.70 (P=O), 65.82 (PPh_3). $^{13}C\{^1H\}$ NMR (50.3 MHz, CD_2Cl_2): δ 18.50 (d, $^1J_{CP}$ = 67.60 Hz, CH_2PCH_2), 128-136 (Ph), 208.68 (CO) and 213.58 (CO). ^1H NMR (200.1 MHz, CD_2Cl_2): δ 1.18 (d, $^2J_{HH}$ = 15.20 Hz, 2H, CH*H*PCH*H*), 2.32 (t, $^2J_{HH} = {}^2J_{HP}$ = 15.20 Hz, 2H, C*H*HPC*H*H), 6.80-7.80 (m, 20H, Ph).

Complex 3. Complex **1** (40 mg, 0.081 mmol) was treated with $Me_3NO{\cdot}2H_2O$ (9 mg, 0.081 mmol) and $P(OEt)_3$ (14 µL, 0.082 mmol) according to the general method. Anal. Calcd for $C_{19}H_{24}Fe_2O_9P_2S_2$: C, 35.70; H, 4.57; S, 10.03. Found: C, 35.30; H, 4.49; S 9.88. Micro-ESI-MS (*m*/*z*): 656.8 $[M + Na]^+$. IR (CH_2Cl_2): 1946, 1983, 2003, 2058 cm^{-1}. $^{31}P\{^1H\}$ NMR (CD_2Cl_2, 161.95 MHz): δ 30.70 (P=O), 170 ($P(OEt)_3$). $^{13}C\{^1H\}$ NMR (50.3 MHz, CD_2Cl_2): δ 16.4 (d, $^3J_{CP}$ = 6.41 Hz, $P(OCH_2CH_3)_3$), 19.6 (d, $^1J_{CP}$ = 62.09 Hz, CH_2PCH_2), 61.95 (d, $^2J_{CP}$ = 4.58 Hz, $P(OCH_2CH_3)_3$), 128-135 (Ph), 208.84 (CO) and 212.33 (d, $^2J_{CP}$ = 16.30 Hz, CO). ^1H NMR (200 MHz, CD_2Cl_2): δ 1.38 (t, $^3J_{HH}$ = 7.03 Hz, 9H, $P(OCH_2CH_3)_3$), 2.20 (d, $^2J_{HH}$ = 14.70 Hz, 2H, CH*H*PCH*H*), 2.57 (t, $^2J_{HH}$ = 14.70, $^2J_{HP}$ = 15.50 Hz, 2H, C*H*HPC*H*H), 4.21 (q, $^3J_{HH} = {}^3J_{HP}$ = 7.03 Hz, 6H, $P(OCH_2CH_3)_3$), 7.40-7.62 (m, 5H, Ph).

Acknowledgments. L. A. thanks the Deutscher Akademischer Austausch Dienst (DAAD) for scholarship. Provision of computing time by the Ohio Supercomputing Centre, Columbus, OH, USA is gratefully acknowledged.

Supporting Information Available. Crystallographic data deposited at the Cambridge Crystallographic Data Centre under CCDC-1030468 for **2**, and CCDC-1030469 for **3** contain the supplementary crystallographic data excluding structure factors; this data can be obtained free of charge

via www.ccdc.cam.ac.uk/conts/retrieving.html (or from the Cambridge Crystallographic Data Centre, 12, Union Road, Cambridge CB2 1EZ, UK; fax: (+44) 1223-336-033; or deposit@ccdc.cam.ac.uk). Variable temperature $^{31}P\{^{1}H\}$ NMR spectra at 400 MHz of complex **3** in MeOD (Figure S1). Cyclic voltammetry of complex **1** (CH_2Cl_2/NBu_4PF_6 solution) at different scan rates (Figure S2). Plots of the cathodic current (I_p^c) versus square root of scan rate for complex **1** (Figure S3). Figure S4 shows the cyclic voltammetry of $O{=}PPh(CH_2Cl)_2$ CH_2Cl_2/NBu_4PF_6 solution at 0.2 $V{\cdot}s^{-1}$. Figure S5 shows the Cyclic voltammetry of complex **2** (CH_2Cl_2/NBu_4PF_6 solution) at various scan rates. Calculated structures for the neutral and the reduced species of **5** (Figure S6) and **6** (Figure S7). Calculated structures as well as results of DFT calculations for the neutral and the reduced species of **1** (Figure S8) and **3** (Figure S9). Results of DFT calculations of **1** and **3**. Discussion of the DFT calculations of **P** (Figure S10) and its oxidation products (Figure S11). Results of DFT calculations of **5** and **6** in the neutral, monoanionic and dianionic state as well as **P1**, **P2** and the reduced species derived from them (Table 1). Tables giving optimized Cartesian coordinates of the calculated species are shown. Copies of the data can be obtained free of charge on application to CCDC, 12 Union Road, Cambridge CB2 1EZ, UK [E-mail: deposit@ccdc.cam.ac.uk].

References

(1) Adams, M. W.; *Biochim. Biophys. Acta* **1990**, *1020*, 115-145.

(2) Frey, M.; *ChemBioChem* **2002**, *3*, 153-160.

(3) (a) Cammack, R.; *Nature.* **1999**, *397*, 214-215. (b) Vignais, P. M.; Billoud, B.; *Chem. Rev.* **2007**, *107*, 4206-4272. (c) Fontecilla-Camps, J. C.; Volbeda, A.; Cavazza, C.; Nicollet, Y.; *Chem. Rev.* **2007**, *107*, 4273-4303. (d) De Lacey, A. L. ; Fernandez, V. M. ; Rousset, M.; Cammack, R.; *Chem. Rev.* **2007**, *107*, 4304-4330.

(4) Holm, R. H.; Kennepohl, P.; Solomin, E. I.; *Chem. Rev.* **1996**, *96*, 2239-2314.

(5) Adams, M. W.; Mortenson, L. E.; *J. Bio. Chem.* **1984**, *259*, 7045-7055.

(6) (a) Tard, C.; Pickett, C.; *Chem. Rev.* **2009**, *109*, 2245-2274. (b) Roy, S.; Shinde, S.; Hamilton, G. A.; Hartnett, H. E.; Jones, A. K.; *Eur. J. Inorg. Chem.* **2011**, 1050-1055. (b) Gao, W.; Song, Li-C.; Yin, B- S.; Zan, H- N.; Wang, D- F.; Song, H- B.; *Organometallics* **2011**, *30*, 4097-4107. (c) Durgaprasad, G.; Bolligarla, R.; Das, S. K.; *J. Organomet. Chem.* **2012**, *706-707*, 37-45. (d) Topf, C.; Monkowius, U.; Knör, G.; *Inorg. Chem. Commun.* **2012**, *21*, 147-150.

(7) Peters, J. W.; Lanzilotta, W. N.; Lemon, B. J.; Seefeldt, L. C. *Science*. 1998, *282*, 1853-1858.

(8) Nicolet, Y.; Piras, C.; Legrand, P.; Hatchikian, C. E.; Fontecilla-Camps, J. C.; *Structure* **1999**, *7*, 13-23.

(9) (a) A. Adamska, A. Silakov, C. Lambertz, O. Rüdiger, T. Happe, E. Reijerse, W. Lubitz, *Angew. Chem*. **2012**, *124*, 11624-11629. (b) H. -J. Fan, M. B. Hall, *J. Am. Chem. Soc*. **2001**, *123*, 3828-3829.

(10) (a) Galinato, M. G. I.; Whaley, M. W.; Roberts, D.; Wang, P.; Lehnert, N.; *Eur. J. Inorg. Chem.* **2011**, 1147-1154. (b) Liu, C.; Peck, J. N. T.; Wright, J. A.; Pickett, C. J.; Hall, M. B.; *Eur. J.*

Inorg. Chem. **2011**, 1080-1093. (c) Zhou, T.; Liu, Y. Mo. A.; Zhou, Z.; Tsai, K. R.; *Inorg. Chem.* **2004**, *43*, 923-930. (d) Zampella, G.; Greco, C.; Fantucci, P.; Gioia, L. De; *Inorg. Chem.* **2006**, *45*, 4109-4118. (e) Wang, Z.; Jiang, W.; Liu, J.; Jiang, W.; Wang, Y.; Åkermark, B.; Sun, L.; *J. Organomet. Chem.* **2008**, *693*, 2828-2834. (f) Wright, J. A.; Pickett, C. J.; *Chem. Comm.* **2009**, 5719-5721.

(11) (a) Nicolet, Y.; Lacey, A. L. de; Vernede, X.; Fernandez, V. M.; Hatchikian, C. E.; Fontecilla-Camps, J. C. *J. Am. Chem. Soc.* **2001**, *123*, 1596-1602. (b) Nicolet, Y.; Lemon, B. J.; Fontecilla-Camps, J. C.; Peters, J. W. *Trends Biochem. Sci.* **2000**, *25*, 138-143. (c) Nicolet, Y.; Cavazza, C.; Fontecilla-Camps, J. C. *J. Inorg. Biochem.* **2002**, *91*, 1-8.

(12) Lubitz, W.; Ogata, H.; Rüdiger, O.; Reijerse, E. *Chem. Rev*. **2014**, *114*, 4081-4148.

(13) Zsolnai, L.; Huttner, G. *Z. Naturforsch*., **1982**, *37b*, 1430-1436.

(14) (a) Wang, Z.; Liu, J. -H.; He, C. -J.; Jiang, S.; Åkermark, B.; Sun. L. –C. *Journal of Organometallic Chemistry* **2007**, *692*, 5501-5507. (b) Si, G.; Wang, W. -G.; Wang, H. -Y.; Tung, C. -H.; Wu, L. -Z.; *Inorg. Chem.* **2008**, *47*, 8101-8111. (c) Si, G.; Wang, W. -G.; Ding, J.; Shan, X. -F.; Zhao, Y. -P.; Tung, C. -H.; Xu, M. *Tetrahedron Lett.* **2007**, *48*, 4775-4779.

(15) Song, L. -C.; Yang, Z. -Y.; Bian, H. -Z.; Liu, Y.; Wang, H. -T.; Liu, X. -F.; Hu Q. -M. *Organometallics* **2005**, *24*, 6126-6135.

(16) (a) Windhager, J.; Rudolph, M.; Bräutigam, S.; Görls, H.; Weigand, W. *Eur. J. Inorg. Chem.* **2007**, 2748-2760. (b) Windhager, J.; Görls, H.; Petzold, H.; Mloston, G.; Linti, G.; Weigand, W. *Eur. J. Inorg. Chem*. **2007**, 4462-4471. (c) Windhager, J.; Seidel, R. A.; Apfel, U. -P.; Görls, H.; Linti, G.; Weigand, W. *Chemistry. Biodiversity*. **2008**, *5*, 2023-2041.

(17) (a) Harb, M. K.; Niksch, T.; Windhager, J.; Görls, H.; Holze, R.; Lockett, L. T.; Okumura, N.; Evans, D. H.; Glass, R. S.; Lichtenberger, D. L.; El-khateeb, M.; Weigand, W. *Organometallics*,

2009*, 28*, 1039-1048. (b) Harb, M. K.; Windhager, J.; Niksch, T.; Görls, H.; Sakamoto, T.; Smith, E. R.; Glass, R. S.; Lichtenberger, D. L.; Evans, D. H.; El-khateeb, M.; Weigand, W. *Tetrahedron* **2012**, *68*, 10592-10599.

(18) (a) Apfel, U. -P.; Troegel, D.; Halpin, Y.; Tschierlei, S.; Uhlemann, U.; Görls, H.; Schmitt, M.; Popp, J.; Dunne, P.; Venkatesan, M.; Coey, Rudolph, M.; Vos, G. J.; Tacke, R.; Weigand, W. *Inorg. Chem.* **2010**, *49*, 10117-10132. (b) Apfel, U. -P.; Halpin, Y.; Görls, H.; Vos, G. J.; Weigand, W. *Eur. J. Inorg. Chem.* **2011**, 581-588. (c) Apfel, U. -P; Görls, H.; Felton, G. A. N.; Evans, D. H.; Glass, R. S.; Lichtenberger, D. L.; Weigand, W. *Helv. Chim. Acta*, **2012***, 95*, 2168-2175.

(19) (a) Razavet, M.; Davies, S. C.; Hughes, D. L.; Barclay, J. E.; Evans, D. J.; Fairhurst, S. A.; Liu, X.; Pickett, C. J. *Dalton Trans*. **2003**, 586-595. (b) Gloaguen, F.; Lawrence, J. D.; Schmidt, M.; Wilson, S. R.; Rauchfuss, T. B. *J. Am. Chem. Soc*. **2001**, *123*, 12518-12527. (c) Le Cloirec, A.; Best, S. P.; Borg, S.; Davies, S. C.; Evans, D. J.; Hughes, D. L.; Pickett, C. J. *Chem. Commun*. **1999**, 2285-2286.

(20) (a) Song, L. -C.; Li, Q. -L.; Feng, Z. -H.; Sun, X. -J.; Xie, Z. -J.; Song, H. -B. *Dalton Trans*., **2013**, *42*, 1612-1626. (b) Thomas, C. M.; Rudiger, O.; Liu, T.; Carson, C. E.; Hall, M. B.; Darensbourg, M. Y. *Organometallics*, **2007**, *26*, 3976-3984. (c) Singleton, M. L.; Jenkins, R. M.; Klemashevich, C. L.; Darensbourg, M. Y. *C.R. Chimie*, **2008**, *11*, 861-874. (d) Ezzaher, S.; Capon, J. -F.; Gloaguen, F.; Petillon, F. Y.; Schollhammer, P.; Talarmin, J. *Inorg. Chem*., **2009**, *48*, 2-4. (e) Li, P.; Wang, M.; He, C.; Liu, X.; Jin, K.; Sun, L. *Eur. J. Inorg. Chem.*, **2007**, 3718-3727. (f) Morvan, D.; Capon, J. -F.; Gloaguen, F.; Schollhammer, P. Talarmin, J. *Eur. J. Inorg. Chem.*, **2007**, 5062-5068. (g) Thomas, C. M.; Rudiger, O.; Liu, T.; Carson, C. E.; Hall, M. B.; Darensbourg, M. Y. *Organometallics*, **2007**, *26*, 3976-3984. (h) Gao, W.; Ekstrom, J.; Liu, J.; Chen, C.; Eriksson, L.; Weng, L.; Åkermark, B.; Sun, L. *Inorg. Chem.*, **2007**, *46*, 1981-1991. (i) Song, L. -C.; Li, C. -G.; Ge, J. -H.; Yang, Z. -Y.; Wang, H. -T.; Zhang, J.; Hu, Q. -M. *J. Inorg.*

Biochem., **2008**, *102*, 1973-1979. (j) Ezzaher, S.; Capon, J. -F.; Gloaguen, F.; Petillon, F. Y.; Schollhammer, P.; Talarmin, J. *Inorg. Chem.* **2007**, *46*, 9863-9872. (k) Wang, Z.; Liu, J. -H.; He, C. -J.; Jiang, S.; Åkermark, B.; Sun, L. -C. *J. Organomet. Chem.*, **2007**, *692*, 5501-5507. (l) Zaffaroni, R.; Rauchfuss, T. B.; Gray, D. L.; De. Gioia, L.; Zampella, G. *J. Am. Chem. Soc*. **2012**, *134*, 19260-19269. (m) Jablonskytė, A.; Wright, J. A.; Pickett, C. J. *Eur. J. Inorg. Chem.* **2011**, 1033-1037. (n) Liu, Y. -C.; Lee, C. -H.; Lee, G. -H.; Chiang, M. -H. *Eur. J. Inorg. Chem*. **2011**, 1155-1162.

(21) (a) Tye, J. W.; Lee, J.; Wang, H. -W.; Mejia-Rodriguez, R.; Reibenspies, J. H.; Hall, M. B.; Darensbourg, M. Y. *Inorg. Chem.* **2005**, *44*, 5550-5552. (b) Thomas, C. M.; Liu, T.; Hall, M. B.; Darensbourg, M. Y. *Inorg. Chem.* **2008**, *47*, 7009-7024. (c) Li, T.; Darensbourg, M. Y. *J. Am. Chem. Soc.*, **2007**, *129*, 7008-7009. (d) Hou, J.; Peng, X.; Liu, J.; Gao, Y.; Zhao, X.; Gao, S.; Han, K. *Eur. J. Inorg. Chem*. **2006**, 4679-4686.

(22) (a) Hsieh, C. -H.; Erdem, Ö- F.; Harman, S. D.; Singleton, M. L.; Reijerse, E.; Lubitz, W.; Popescu, C. V.; Reibenspies, J. H.; Brothers, S. M.; Hall, M. B.; Darensbourg. M. Y. *J. Am. Chem. Soc.* **2012**, *134*, 13089-13102. (b) Justice, A. K.; Rauchfuss, T. B.; Wilson. S. R.; *Angew. Chem. Int. Ed.* **2007**, *46*, 6152-6154. (c) Olsen, M. T.; Bruschi, M.; De Gioia, L.; Rauchfuss, T. B.; Wilson, S. R. *J. Am. Chem. Soc.* **2008**, *130*, 12021-12030.

(23) (a) Razavet, M.; Davies, S. C.; Hughes, D. L.; Barclay, J. E.; Evans, D. J.; Fairhurst, S. A.; Liu, X.; Pickett, C. J. *Dalton Trans*. **2003**, 586-595. (b) Hu, M. -Q.; Ma, C. -B.; Si, Y. -T.; Chen, C. -N.; Liu, Q. -T. *J. Inorg. Biochem.* **2007**, *101*, 1370-1375. (c) Razavet, M.; Davies, S. C.; Hughes, D. L.; Pickett, C. J.; *Chem.Commun*. **2001**, 847-848. (d) Lawrence, J. D.; Li, H.; Rauchfuss, T. B.; *Chem. Commun.* **2001**, *16*, 1482-1483. (e) Song, L. -C.; Yang, Z. -Y.; Bian, H. -Z.; Hu, Q. -M. *Organometallics* **2004**, *23*, 3082-3084. (f) Daraosheh, A. Q.; Harb, M. K.; Windhager, J.; Görls, H.; El-khateeb, M.; Weigand, W.; *Organometallics* **2009**, *28*, 6275-6280.

(24) Tschierlei, S.; Ott, S.; Lomoth, R. *Energy Environ. Sci.* **2011**, *4*, 2340-2352.

(25) Stanley, J. L.; Heiden, Z. M.; Rauchfuss, T. B.; Wilson, S. R.; De Gioia, L.; Zampella, G. *Organometallics* **2008**, *27*, 119-125.

(26) (a) Munery, S.; Capon, J. -F.; De Gioia, L.; Elleouet, C.; Greco, C.; Pétillon, F. Y.; Schollhammer, P.; Talarmin, J.; Zampella, G. *Chem. Eur. J.* **2013**, *19*, 15458-15461. (b) Wang, W.; Rauchfuss, T. B.; Moore, C. E.; Rheingold, A. L.; De Gioia, L.; Zampella, G. *Chem. Eur. J.* **2013**, *19,* 15476-15479.

(27) Almazahreh, L. R.; Apfel, U. -P.; Imhof, W.; Rudolph, M.; Görls, H.; Talarmin, J.; Schollhammer, P.; El-khateeb, M.; Weigand, W. *Organometallics*, **2013**, *32*, 4523-4530.

(28) (a) Capon, J. -F.; Ezzaher, S.; Gloaguen, F.; Pétillon, F. Y.; Schollhammer, P.; Talarmin, J.; Davin, T. J.; McGrady, J. E.; Muir, K. W. *New J. Chem.* **2007**, *31*, 2052-2064. (b) Felton, G. A. N.; Petro, B. J.; Glass, R. S.; Lichtenberger, D. L.; Evans, D. H. *J. Am. Chem. Soc.* **2009**, *131*, 11290-11291. (c) Felton, G. A. N.; Vannucci, A. K.; Chen, J.; Lockett, L. T.; Okumura, N.; Petro, B. J.; Zakai, U. I.; Evans, D. H.; Glass, R. S.; Lichtenberger, D. L. *J. Am. Chem. Soc.* **2007**, *129*, 12521-12530.

(29) Crouthers, D. J.; Denny, J. A.; Bethel, R. D.; Munoz, D. G.; Darensbourg, M. Y. *Organometallics* **2014**, *33*, 4747-4755.

(30) Windhager, J.; Apfel, U. -P.; Yoshino, T.; Nakata, N.; Görls, H.; Rudolph, M.; Ishii, A.; Weigand, W. *Chem. Asian J.* **2010**, *5*, 1600-1610.

(31) (a) Durgaprasad, G.; Das, S. K. *J. Organomet. Chem.* **2012**, *717*, 29-40. (b) Li, P.; Wang, M.; He, C.; Li, G.; Liu, X.; Chen, C.; Åkermark, B.; Sun, L. *Eur. J. Inorg. Chem.* **2005**, 2506-2513. (c) Durgaprasad, G.; Bolligarla, R.; Das, S. K. *J. Organomet. Chem.*, **2011**, *696*, 3097-3105.

(32) (a) -Lin Su, W.; -P. H.; Huang, Chen, W. -T.; Hsu, W. -Y.; Chang, H. -Y.; Ho, S. -Y.; Wanga, S. -P.; Shyu, S. -G. *J. Chin. Chem. Soc.* **2011**, *58*, 163-173. (b) R. H. Crabtree, Wiley, **2009**, Ed fifth, pp. 99-102. (c) R. H. Crabtree, Wiley, **2009**, Ed fifth, pp. 203-204.

(33) Lyon, E. J.; Georgakaki, I. P.; Reibenspies, J. H.; Darensbourg, M. Y. *Angew. Chem., Int. Ed*. **1999**, *38*, 3178-3180.

(34) (a) Tolman, C. A.; *Chemical Reviews* **1977**, *77*, 313-348. (b) Bunten, K. A.; Chen, L. Z.; Fernandez, A. L.; Poe, A. J. *Coord. Chem. Rev*. **2002**, *233*, 41-51. (c) Tolman, C. A.; *J. Am. Chem. Soc.* **1970**, *92*, 2953-2956.

(35) Charreteur, K.; Kdider, M.; Capon, J. -F.; Gloaguen, F.; Pétillon, F. Y.; Schollhammer, P.; Talarmin, J. *Inorg. Chem.* **2010**, *49*, 2496-2501.

(36) Lever, A. B. P. *Inorg. Chem.* **1990**, *29*, 1271-1285.

(37) (a) Darensbourg, D. J.; Graves, A. H. *Inorg. Chem*. **1979**, *18*, 1257-1261. (b) Wovkulich, M. J.; Atwood, J. D. *Organometallics* **1982**, *1*, 1316-1321. (c) Atwood, J. D.; Wovkulich, M. J.; Sonnenberger, D. C. *Acc. Chem. Res.* **1983**, *16*, 350-355. (d) Almazahreh, L.; El-khateeb, M.; Harb, M.; Görls, H.; Weigand, W. *Transition Met Chem*. **2013**, *38*, 377–383.

(38) (a) Fernandes, J. B.; Zhang, L. Q.; Schultz, F. A. *J. Electroanal. Chem.* **1991**, *297*, 145-161. (b) Uhrhammer, D.; Schultz, F. A. *J. Phys. Chem.* A, **2002**, *106*, 11630-11636. (c) Gao, S.; Fan, J.; Sun, S.; Song, F.; Peng, X.; Duan, Q.; Jianga, D.; Liang, Q. *Dalton Trans.* **2012**, *41*, 12064-12074.

(39) Frisch, M. J.; Trucks, G. W.; Schlegel, H. B.; Scuseria, G. E.; Robb, M. A.; Cheeseman, J. R.; Scalmani, G.; Barone, V.; Mennucci, B.; Petersson, G. A.; Nakatsuji, H.; Caricato, M.; Li, X.; Hratchian, H. P.; Izmaylov, A. F.; Bloino, J.; Zheng, G.; Sonnenberg, J. L.; Hada, M.; Ehara, M.; Toyota, K.; Fukuda, R.; Hasegawa, J.; Ishida, M.; Nakajima, T.; Honda, Y.; Kitao, O.;

Nakai, H.; Vreven, T.; Montgomery, Jr., J. A.; Peralta, J. E.; Ogliaro, F.; Bearpark, M.; Heyd, J. J.; Brothers, E.; Kudin, K. N.; Staroverov, V. N.; Keith, T.; Kobayashi, R.; Normand, J.; Raghavachari, K.; Rendell, A.; Burant, J. C.; Iyengar, S. S.; Tomasi, J.; Cossi, M.; Rega, N.; Millam, J. M.; Klene, M.; Knox, J. E.; Cross, J. B.; Bakken, V.; Adamo, C.; Jaramillo, J.; Gomperts, R.; Stratmann, R. E.; Yazyev, O.; Austin, A. J.; Cammi, R.; Pomelli, C.; Ochterski, J. W.; Martin, R. L.; Morokuma, K.; Zakrzewski, V. G.; Voth, G. A.; Salvador, P.; Dannenberg, J. J.; Dapprich, S.; Daniels, A.D.; Farkas, O.; Foresman, J. B. Ortiz, J. V. Cioslowski, J.; Fox, D. J.; Gaussian, Inc., Wallingford CT, **2010**.

(40) (a) Becke, A. D. *J. Chem. Phys*. **1993**, *98*, 5648. (b) Lee, C.; Yang, W. W.; Parr, R. G. *Phys. Rev.* 1988, *B37*, 785-789.

(41) (a) Dolg, M.; Stoll, H.; Preuss, H. *Theor. Chim. Acta*. **1993**, *85*, 441-450. (b) Bergner, A.; Dolg, M.; Küchle, W.; Stoll, H.; Preuss, H. *Mol. Phys*. **1993**, *80*, 1431-1441.

(42) (a) Thomas, C. M.; Darensbourg, M. Y.; Hall, M. B. *J. Inorg. Biochem*. **2007**, *101*, 1752-1757. (b) Zampella, G.; Fantucci, P.; De Gioia, L. *Chem. Commun*. **2010**, *46*, 8824-8826. (c) Song, L. -C.; Xie, Z. -J.; Liu, X. -F.; Ming, J. -B.; Ge, J. -H.; Zhang, X. -G.; Yan, T. -Y.; Gao, P. *Dalton Trans*. **2011**, *40*, 837-846. (d) Stiebritz, M. T.; Finkelmann, A. R.; Reiher, M. *Eur. J. Inorg. Chem*. **2011**, 1163-1171. (e) Chouffai, D.; Zampella, G.; Capon, J. -F.; De Gioia, L.; Gloaguen, F.; Petillon, F. Y.; Schollhammer, P.; Talarmin, J. *Inorg. Chem*. **2011**, *50*, 12575-12585. (f) Kania, R.; Frederix, P. W. J. M.; Wright, J. A.; Ulijn, R. V.; Pickett, C. J.; Hunt, N. T. *J. Chem. Phys*. **2012**, *136*, 044521/1-044521/9. (g) Leidel, N.; Chernev, P.; Havelius, K. G. V.; Schwartz, L.; Ott, S.; Haumann, M. *J. Am. Chem. Soc*. **2012**, *134*, 14142-14157.

(43) COLLECT, Data Collection Software; Nonius B. V., The Netherlands **1998**.

(44) Otwinowski Z.; Minor, W. „Processing of X-Ray Diffraction Data Collected in Oscillation Mode“, in Methods in Enzymology, Vol. 276, Macromolecular Crystallography, Part A, edited by C.W. Carter & R.M. Sweet, pp. 307-326, Academic Press, San Diego, USA, **1997**.

(45) SADABS 2.10, Bruker-AXS inc., **2002**, Madison, WI, U.S.A.

(46) Sheldrick, G. M. *Acta Cryst.* **2008**, *A46*, 112-122.